 https://doi.org/10.3311/PPee.21912

Periodica Polytechnica Electrical Engineering and Computer Science, 68(3), pp. 246–255, 2024

PV System Linked to an Electrical Network with an Active Power Filter Using DPC Modified Method Under Distorted Grid Voltage Conditions

Kamel Djazia[1*], Mustapha Sarra[2]

[1] Department of Electronics, Faculty of Technology, University of M'sila, 28000 M'sila, P.O.B. 166, Algeria
[2] Department of Electronics, Faculty of Technology, University of Bordj Bou Arreridj, 34030 Bordj Bou Arreridj El-Anasser, P.O.B. 64, Algeria
[*] Corresponding author, e-mail: kamel.djazia@univ-msila.dz

Received: 22 January 2023, Accepted: 06 September 2023, Published online: 11 December 2023

Abstract

This article presents an energy system that enhances the quality of electrical energy by injecting photovoltaic (PV) renewable energy into the electrical network in the presence of a polluting load. This system is based on a new control approach known as Zero Direct Power Command (ZDPC). The innovative aspect of the proposed work is the addition of clean energy while simultaneously removing the unsettling harmonics produced by the nonlinear loads provided by distorted voltages. This approach combines a traditional Proportional Integrator (PI) controller for regulating the DC bus voltage with a clever technique (fuzzy logic) for tracking the Maximum Power Point Tracking (MPPT). The current has a harmonic distortion rate of about 1% with unity power factor due to the suppression of undesirable harmonics from the source currents. A PV panel connected in series with a chopper and managed by fuzzy logic via a two-state inverter ensures the injection of PV energy into the electrical network. Software called MATLAB/Simulink is used to model this system. The outcomes demonstrate the reliability and viability of the ZDPC control, which concurrently ensures harmonic current compensation, power factor correction, and the introduction of solar power into the electrical network despite distorted source voltages.

Keywords

active power filter, ZDPC, PV, fuzzy logic, MPPT

1 Introduction

Photovoltaic (PV) systems seem to be well established as a means of converting PV energy into electrical energy. The extraction of the maximum system power called Maximum Power Point Tracking (MPPT) strategy allows an efficient way to solve the optimization problem. The vector Pulse-Width Modulation (PWM) control is used to synchronize the output power of the inverter with that injected into the network. Several MPPT algorithms, such as incremental conductance (IC), perturb and observe (PO), and escalation (HC) have been proposed [1]. The tracking algorithm, based on fuzzy logic, is considered one of the most efficient algorithms [1–3]. In our research, the Maximum Power Point (MPP) is reached intelligently regardless of the degree of variation in solar radiation due to the fuzzy MPPT technique [2].

Semiconductor-based loads are non-linear loads that absorb non-sinusoidal currents, even if they are supplied with a sinusoidal voltage, they therefore behave as harmonic generators and also exchange reactive energy. Clearly, this harmonic phenomenon deserves to be taken into consideration and seriously given the many anomalies that they can produce. To reduce or eliminate these disturbances and thus improve the quality of the distributed energy, several solutions exist [4-6], such as the proposed method of the active power filter based on the new command called Zero Direct Power Command (ZDPC) [4].

This article is both the subject of studying the injection of clean energy from the PV system to the electrical network and the improvement of the energy polluted by the non-linear loads connected to the networks.

This article is organized as follows; Section 2 presents the principle of the photovoltaic generator (PVG) based on a fuzzy control of the MPPT. Section 3 discusses the detailed operating principle of the proposed ZDPC method.

The results of the simulation are taken under unfavorable conditions (distorted network voltage). At the end, we conclude the article.

Cite this article as: Djazia, K., Sarra, M. "PV System Linked to an Electrical Network with an Active Power Filter Using DPC Modified Method Under Distorted Grid Voltage Conditions", Periodica Polytechnica Electrical Engineering and Computer Science, 68(3), pp. 246–255, 2024.
https://doi.org/10.3311/PPee.21912

2 Photovoltaic generator

PV solar energy results from the direct transformation of sunlight into electrical energy by means of cells generally based on crystalline silicon, which remains the most technologically and industrially advanced sector. Solar electricity is an important source of renewable energy which could be an alternative to other conventional sources in order to satisfy the large energy needs in the future [7, 8].

2.1 The photovoltaic effect

The PV effect is a physical phenomenon specific to certain materials called "semiconductors" which, when exposed to light, produce electricity.

2.2 Operating principle

Fig. 1 illustrates a typical PV cell where its constitution is detailed. A PV cell is made from two layers of silicon, one P-doped (boron-doped) and the other N-doped (phosphorus-doped) thereby creating a PN junction with a barrier of potential.

When the photons are absorbed by the semiconductor, they transmit their energy to the atoms of the PN junction in such a way that the electrons of these atoms are freed and create electrons (N charges) and holes (P charges). This then creates a difference in potential between the two layers. This difference in potential is measurable between the connections of the positive and negative terminals of the cell.

2.3 Electrical characteristics of a photovoltaic cell

Fig. 2 shows the equivalent circuit of a PV cell under illumination. It corresponds to an I_{ph} current generator mounted in parallel with a diode. Two parasitic resistors are introduced in this diagram.

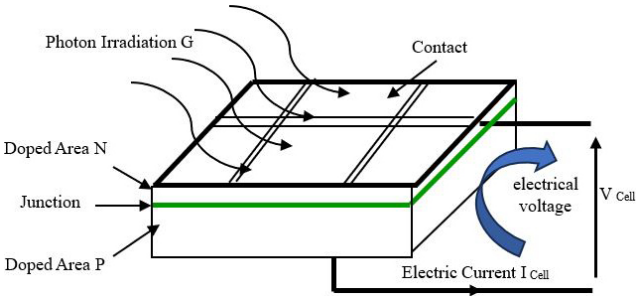

Fig. 1 Operating principle

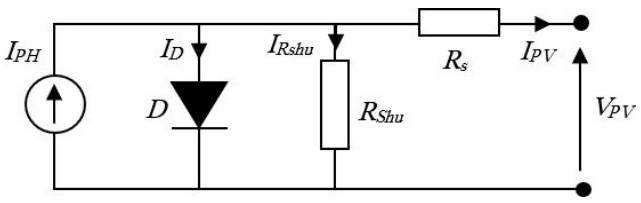

Fig. 2 Electrical equivalent diagram of the PV cell

These resistors have some influence on the characteristic $I = f(V)$ of the cell [3]:

- the series resistor (R_s) is the internal resistance of the cell; it depends mainly on the resistance of the semiconductor used, on the contact resistor of the collector grids and on the resistivity of these grids;
- the shunt resistor (R_{shu}) is due to a leakage current at the junction; it depends on the way in which this was carried out.

The mathematical model for the current-voltage characteristic of a PV cell is given by Eq. (1):

$$I_{pv} = I_{ph} - I_{sat}\left[e^{\frac{q\times(V_{pv}+I_{pv}\times R_s)}{nKT}} - 1\right] - \frac{V_{pv} + I_{pv}\times R_s}{R_{shu}}, \quad (1)$$

where I_{sat} is the saturation current, K is the Boltzmann constant (1.381×10^{-23} J/K), T is the effective cell temperature in Kelvin (K), q is the charge of the electron ($q = 1,6 \times 10^{-19}$ C), n is the ideality factor of the junction ($1 < n < 3$), I_{pv} is the current supplied by the cell when it operates as a generator, V_{pv} is the voltage across the terminals of this same cell, I_{ph} is the photo-current of the cell depending on the illumination and the temperature or else (short circuit) current, R_{shu} is the shunt resistor characterizing the junction leakage currents, R_s is the series resistor representing the various contact and connection resistances [9, 10].

2.4 Maximum power point

The power supplied to the external circuit by a PV cell under illumination depends on the load resistance (external resistance placed at the terminals of the cell). This power is maximum (denoted P_{max}) for an operating point P_{max} (I_{max}, V_{max}) of the current-voltage curve [10].

This maximum power (P_{max}) can be determined by plotting on the same graph the characteristic IV and the constant power hyperbolas. The optimal operating point corresponds to the tangency point of the two curves as shown in Fig. 3 The maximum power delivered to the load is given by Eq. (2):

$$P_{max} = I_{max} \times V_{max}. \quad (2)$$

2.5 Fuzzy logic MPPT controller design

Fuzzy logic is a type of artificial intelligence technology that replicates human reasoning. The researcher of [11] pio-

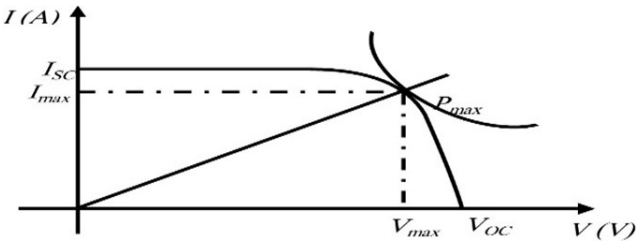

Fig. 3 MPP of a cell

neered the essential concepts of this theory. This approach is employed in our study for the MPPT of a PV module under all-weather situations since it does not need knowledge of mathematical models of linear and nonlinear controlled systems. The fuzzy logic approach is used to track the MPP of a PV module in order to achieve excellent efficiency under all-weather circumstances. The fuzzy logic technique is particularly efficient for both linear and nonlinear controlled systems, and it does not require a formal model. For the MPPT tracking method, the establishment of a fuzzy logic controller (FLC) is realized in three essential steps: fuzzification, inference with rule bases and defuzzification [2, 3, 11, 12], as shown in Fig. 4. During fuzzification, the numerical input quantities are converted into fuzzy variables, while the inference stage determines the controller output decision via the maximum-minimum technique, developed by Mamdani [12], according to the set belonging to the rule bases. The defuzzification step provides in real quantity the incremental duty cycle $\Delta\alpha$. The search pattern is performed by adjusting the duty cycle of the boost, depending on the variation of the following two inputs e and Δe:

$$e(K)=\frac{P_{pv}(K)-P_{pv}(K-1)}{V_{pv}(K)-V_{pv}(K-1)}, \tag{3}$$

$$\Delta e=e(K)-e(K-1), \tag{4}$$

where P_{PV} (K), P_{PV} $(K–1)$, V_{PV} (K), V_{PV} $(K–1)$ are respectively: the power and the voltage PV, captured at two sampling instants K and $(K–1)$.

The output variable is the cyclic ratio $\Delta\alpha(K)$. The variables $\Delta P_{pv}(K)$ and $\Delta V_{pv}(K)$ are given by the Eqs. (5) and (6) [3]:

$$\Delta P_{pv}(K)=P_{pv}(K)-P_{pv}(K-1), \tag{5}$$

$$\Delta V_{pv}(K)=V_{pv}(K)-V_{pv}(K-1), \tag{6}$$

where, at the MPP of the PV generator, $\Delta P_{pv}(K)$ and $\Delta V_{pv}(K)$ are zero. The rule bases of the fuzzy MPPT algorithm rely on the two input variables ($\Delta P_{pv}(K)$, $\Delta V_{pv}(K)$) and on the output variable ($\Delta\alpha$). The $\Delta P_{pv}(K)$ and the $\Delta V_{pv}(K)$ are divided into five denoted fuzzy sets: Negative Big (*NB*), Negative Small (*NS*), Zero (*Z*), Positive Small (*PS*) and Positive Big (*PB*). The rule bases relate the fuzzy inputs to the fuzzy output by the master syntax rule: "*If: A is ... and B is ...*, *Then: C is ...*". According to Table 1 [3], grouping together all the possible relationships between the inputs and the output of the developed controller, we can give the following example*: if:* ΔP_{pv} *is PB and* ΔV_{pv} *is NB then:* $\Delta\alpha$ *is NS*. The choice of the shape of the membership functions of the proposed controller is of the triangular type. The center of gravity method for the defuzzification step is used to calculate the incremental duty cycle $\Delta\alpha$ Eq. (7) [2, 3, 10]. This method calculates the

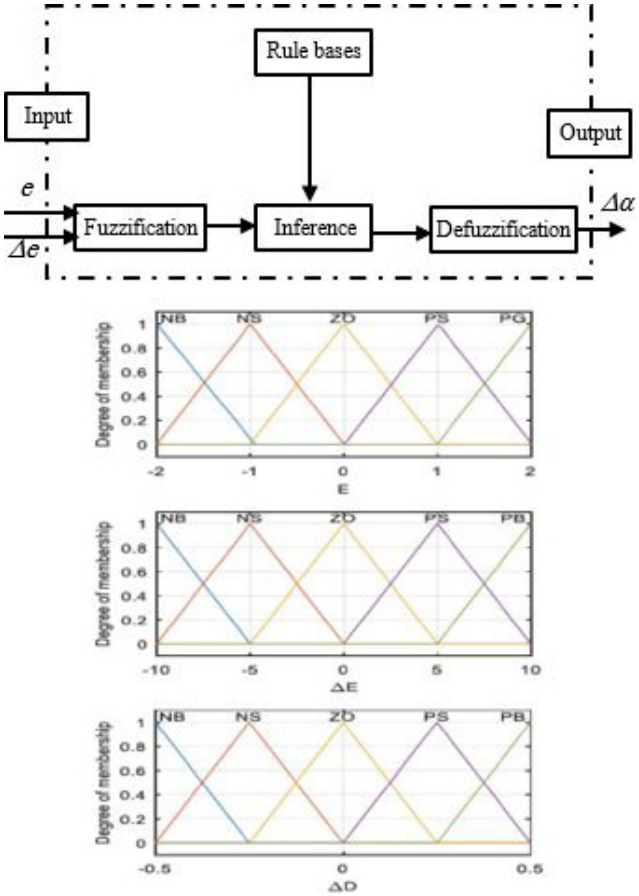

Fig. 4 Principal of fuzzy logic MPPT controller and membership functions

Table 1 Example of a table

$\Delta P\backslash\Delta V$	*NB*	*NS*	*Z*	*PS*	*PB*
NB	*PS*	*PB*	*PB*	*NB*	*NS*
NS	*Z*	*PS*	*PS*	*NS*	*Z*
Z	*Z*	*Z*	*Z*	*Z*	*Z*
PS	*Z*	*NS*	*NS*	*PS*	*Z*
PB	*NS*	*NB*	*NB*	*PB*	*PS*

center of gravity of the final fuzzy space and gives a result which is very related to all the elements of the same fuzzy set. The net value of the control output $\Delta\alpha(K)$ is calculated by Eq. (7). This method provides a crisp value based on the center of gravity of the fuzzy set. The total area of the membership function distribution used to represent the combined control action is divided into a number of sub-areas. The area and the center of gravity or centroid of each sub-area is calculated and then the summation of all these sub-areas is taken to find the defuzzified value for a discrete fuzzy set.

$$\Delta\alpha = \frac{\sum_{j=0}^{n} w_j \Delta\alpha_j}{\sum_{j=0}^{n} w_j} \tag{7}$$

With n the maximum number of effective rules, w represents the weighting factor and $\Delta\alpha_j$ the value corresponding to $\Delta\alpha$. Finally, the duty cycle is obtained by adding this change to the previous value of the control duty cycle as mentioned in Eq. (8) [2, 3, 10]:

$$\alpha(K+1) = \alpha(K) + \Delta\alpha(K). \tag{8}$$

3 The proposed ZDPC principle

Fig. 5 shows the structure of the proposed ZDPC. The principle of ZDPC consists of selecting a sequence of switching orders (S_a, S_b, S_c) of the semiconductors constituting the inverter from a predefined switching table relative to power errors (S_p and S_q) between the instantaneous active and reactive power reference values (p_{ref} and q_{ref}) and the actual values (p and q). Thus, the choice of the optimum switching state is made so that the active power error can be limited within a hysteresis band of width (2HBp) and similarly for the reactive power error with a band of width (2HBq).

To improve performance, the α–β plane is divided into twelve equal sectors of 30°, as illustrated in Fig. 6. Each of the control sequences (S_a, S_b, S_c) corresponds to an input voltage vector at the inverter, $\boldsymbol{v}_i$, whose set is represented in Fig. 5. The DC bus voltage loop is adjusted with a Proportional Integrator (PI) controller. Thus, the active power reference P_{ref} is imposed equal to zero to compensate for harmonics in the source current. While that of reactive power q_{ref} comes from outside. It is imposed equal to zero for absorption of sinusoidal currents under a source voltage of assumed sinusoidal shape to ensure a unit power factor.

The highly selective filter (HSF) filter is used to separate the fundamental and harmonic components of line currents and voltages in order to perform power compensation [4].

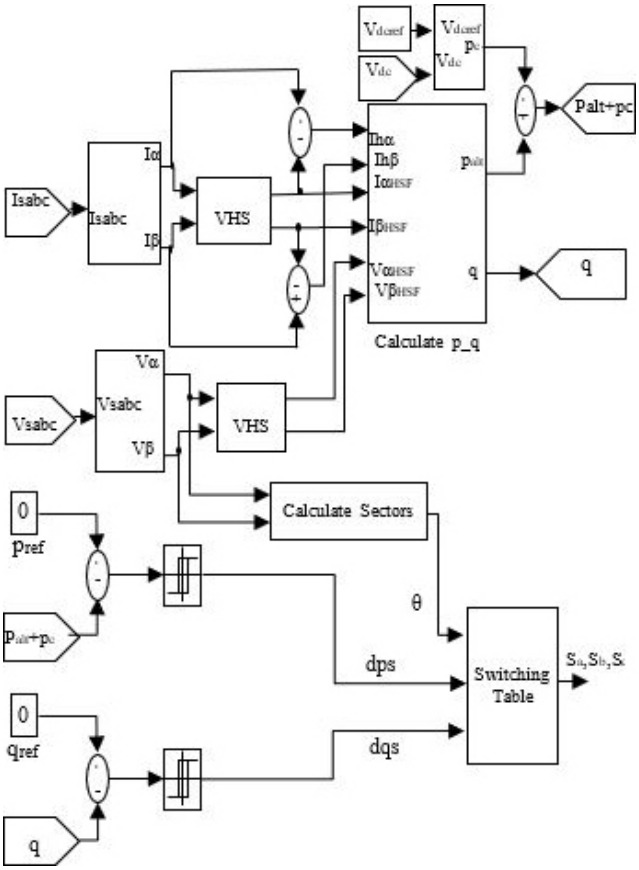

Fig. 5 Synoptic of the ZDPC

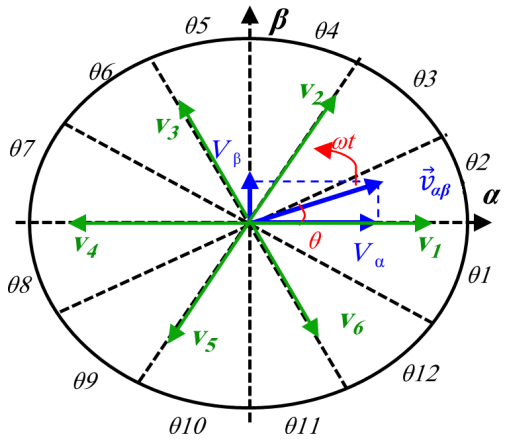

Fig. 6 Representation of the voltage vector in vector space (α, β) divided into twelve (12) sectors

3.1 The choice of sector

The digitized variables d_{ps}, d_{qs} and the position of the network voltage vector (θ), Eq. (10), form a digital word, allowing access to the address of the switch table to select the appropriate control voltage vector. The sector choice block informs us in which domain the actual source voltage vector ($v_{\alpha\beta}$) is located. This position is defined by the following relationship Fig. 6:

$$\theta = arctg\left(\frac{\boldsymbol{v}_\beta}{\boldsymbol{v}_\alpha}\right). \tag{9}$$

The sectors can be expressed numerically as shown in Eq. (10) [4]:

$$(n-2)\times\frac{\pi}{6} \le \theta_n \le (n-1)\times\frac{\pi}{6} \quad n = 1,2,\ldots,12. \tag{10}$$

The Table 2 is predefined, it was first presented by T. Noguchi in 1998 [4]. From Table 2, the vector of voltages to be applied to the input of the inverter is selected ($\boldsymbol{v}_i$) according to the different states of the logical outputs of the established hysteresis comparators and according to the number of the sector where the vector $\boldsymbol{v}_{\alpha\beta}$ is located.

The voltage vector at the input of the MLI inverter, $\boldsymbol{v}_i$, depends on the switching states S_a, S_b and S_c of the semiconductors. According to the different possible combinations of these three states, eight voltage vectors can be applied to the input of the rectifier: two zero vectors named ($\boldsymbol{v}_0$ and $\boldsymbol{v}_7$) and six non-zero vectors ($\boldsymbol{v}_1$, $\boldsymbol{v}_2$, $\boldsymbol{v}_3$, $\boldsymbol{v}_4$, $\boldsymbol{v}_5$, $\boldsymbol{v}_6$). These vectors are represented in the stationary axes α–β as shown in Fig. 6. The six non-zero vectors divide the α–β plane into six sectors each of which is divided into two equal sectors in order to obtain precise control.

The selection of the optimum switching state is done so that power errors can be limited within the hysteresis bands [4, 13–15].

3.2 Hysteresis controller

The main idea of the ZDPC method is to maintain the instantaneous active and reactive power within a desired band. This control is based on two comparators with hysteresis whose input is the error between the reference and estimated values of the active and reactive power [9, 11], given respectively by the Eqs. (11) and (12):

$$\Delta p_s = p_{ref} - p_s, \tag{11}$$

$$\Delta q_s = q_{ref} - q_s. \tag{12}$$

Hysteresis comparators are used to provide two logic outputs d_{ps} et d_{qs}. State "1" corresponds to an increase in the controlled variable (p_s and q_s) while "0" corresponds to a decrease, according to Eqs. (13) and (14):

$$\text{if } \Delta p_s \ge h_p \quad d_{p_s} = 1;\ \text{if } \Delta p_s \le -h_p \quad d_{p_s} = 0, \tag{13}$$

$$\text{if } \Delta q_s \ge h_q \quad d_{q_s} = 1;\ \text{if } \Delta q \le -h_q \quad d_{q_s} = 0, \tag{14}$$

where h_p and h_q are the hysteresis bands.

Table 2 ZDPC switching table

dp	dq	θ_1	θ_2	θ_3	θ_4	θ_5	θ_6	θ_7	θ_8	θ_9	θ_{10}	θ_{11}	θ_{12}
1	0	$\boldsymbol{v}_6$	$\boldsymbol{v}_7$	$\boldsymbol{v}_1$	$\boldsymbol{v}_0$	$\boldsymbol{v}_2$	$\boldsymbol{v}_7$	$\boldsymbol{v}_3$	$\boldsymbol{v}_0$	$\boldsymbol{v}_4$	$\boldsymbol{v}_7$	$\boldsymbol{v}_5$	$\boldsymbol{v}_0$
	1	$\boldsymbol{v}_7$	$\boldsymbol{v}_7$	$\boldsymbol{v}_0$	$\boldsymbol{v}_0$	$\boldsymbol{v}_7$	$\boldsymbol{v}_7$	$\boldsymbol{v}_0$	$\boldsymbol{v}_0$	$\boldsymbol{v}_7$	$\boldsymbol{v}_7$	$\boldsymbol{v}_0$	$\boldsymbol{v}_0$
0	0	$\boldsymbol{v}_6$	$\boldsymbol{v}_1$	$\boldsymbol{v}_1$	$\boldsymbol{v}_2$	$\boldsymbol{v}_2$	$\boldsymbol{v}_3$	$\boldsymbol{v}_3$	$\boldsymbol{v}_4$	$\boldsymbol{v}_4$	$\boldsymbol{v}_5$	$\boldsymbol{v}_5$	$\boldsymbol{v}_6$
	1	$\boldsymbol{v}_1$	$\boldsymbol{v}_2$	$\boldsymbol{v}_2$	$\boldsymbol{v}_3$	$\boldsymbol{v}_3$	$\boldsymbol{v}_4$	$\boldsymbol{v}_4$	$\boldsymbol{v}_5$	$\boldsymbol{v}_5$	$\boldsymbol{v}_6$	$\boldsymbol{v}_6$	$\boldsymbol{v}_1$

$\boldsymbol{v}_1$(100), $\boldsymbol{v}_2$(110), $\boldsymbol{v}_3$(010), $\boldsymbol{v}_4$(011), $\boldsymbol{v}_5$(001), $\boldsymbol{v}_6$(101), $\boldsymbol{v}_0$(000), $\boldsymbol{v}_7$(111)

3.3 IP controller

The ZDPC method must provide DC bus regulation to maintain the capacitor voltage, around the voltage reference ($V_{\mathrm{DC}ref}$). For this purpose, an IP controller is generally used [2, 4]. Fig. 7 shows the simulation model for the controller.

The proportional and integral gain values, K_p and K_i, are given respectively by the Eqs. (15) and (16):

$$K_i = \frac{\omega_n}{2\times\xi}, \tag{15}$$

$$K_p = 2\times C\times\xi\times\omega_n, \tag{16}$$

where:

- ξ: damping ratio ($\xi = 0.707$);
- ω_n: natural pulse.

3.4 The HSF filter

To improve the performance of the classical instantaneous power method, HSF has been implemented, to extract the fundamental component of current and voltage in the synchronous frame without phase shift and amplitude errors. The functional block diagram of HSF is shown in Fig. 8. The transfer function of the filter can be expressed as follows [4, 15]:

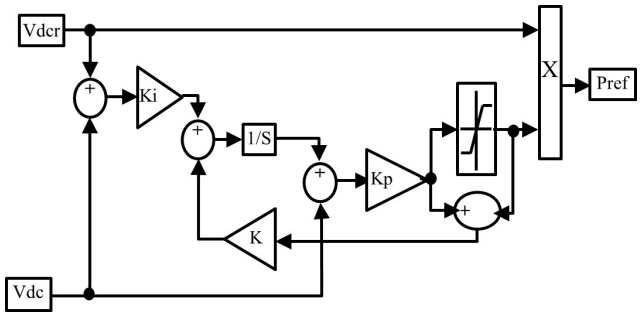

Fig. 7 Simulation model of IP controller

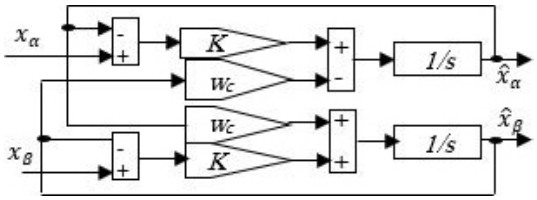

Fig. 8 Block diagram of HSF filter

$$H(s)=\frac{\hat{x}_{\alpha\beta}(s)}{x_{\alpha\beta}}=k\frac{(s+k)+j\omega_c}{(s+k)^2+\omega_c^2}. \tag{17}$$

From the transfer function Eq. (17), we obtain:

$$\hat{x}_\alpha(s)=\frac{K}{s}\left[x_\alpha(s)-\hat{x}_\alpha(s)\right]-\frac{\omega_c}{s}\hat{x}_\beta(s), \tag{18}$$

$$\hat{x}_\beta(s)=\frac{K}{s}\left[x_\beta(s)-\hat{x}_\beta(s)\right]+\frac{\omega_c}{s}\hat{x}_\alpha(s), \tag{19}$$

where the magnitudes and $x_{\alpha\beta}$ represent the output and the input of the filter respectively. They can be $\boldsymbol{v}_{\alpha\beta}$ or $i_{\alpha\beta}$. It is noted that for the pulsation $\omega = \omega_c$, the phase shift introduced by the filter is zero and the gain is unity. We also observe that the decrease in the K value improves the selectivity of HSF. From the HSF output, the AC component of the instantaneous active power can be obtained by Eq. (20) [4, 15]:

$$\tilde{p}=\hat{\boldsymbol{v}}_{\boldsymbol{\alpha}}\times i_{h\alpha}+\hat{\boldsymbol{v}}_{\boldsymbol{\beta}}\times i_{h\beta}, \tag{20}$$

with $i_{h\alpha}$ and $i_{h\beta}$ given respectively by Eqs. (21) and (22):

$$i_{h\alpha}=\left(i_{\alpha d}-\hat{i}_{\alpha d}\right)+\left(i_{\alpha inv}-\hat{i}_{\alpha inv}\right), \tag{21}$$

$$i_{h\beta}=\left(i_{\beta d}-\hat{i}_{\beta d}\right)+\left(i_{\beta inv}-\hat{i}_{\beta inv}\right), \tag{22}$$

where the terms $i_{h\alpha}$ and $i_{h\beta}$ are the harmonic components in the $\alpha\beta$ axis. Whereas instantaneous reactive power is defined by Eq. (23):

$$q_s=\hat{\boldsymbol{v}}_{\boldsymbol{\beta}}\hat{i}_\alpha-\hat{\boldsymbol{v}}_{\boldsymbol{\alpha}}\hat{i}_\beta. \tag{23}$$

Fig. 9 shows the calculation of the disturbing powers $\tilde{p}$ and q_s.

3.5 Generation of control vector

By adding the alternating component ($\tilde{p}$) of the instantaneous active power, linked to both current and voltage disturbances, to the active power p_c, necessary for the regulation of the DC bus, we obtain the disturbing active power p_p which can be expressed through:

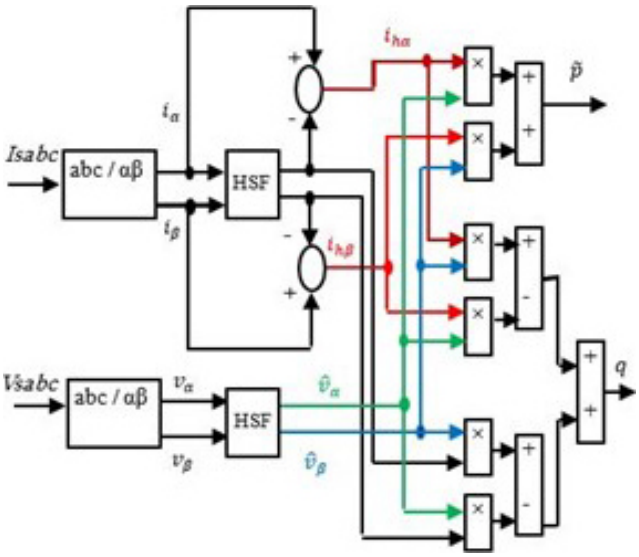

Fig. 9 Computation of v_α, v_β, $\tilde{p}$ and q_s with HSF

$$p_p=\tilde{p}+p_c. \tag{24}$$

To compensate for active and reactive power disturbances (p_p and q_s), a comparison with their zero reference is carried out. The results of the comparison pass through a hysteresis block which generates d_{ps} and d_{qs}. Depending on the sector selected (θ_n) and (d_{ps}, d_{qs}), the appropriate control vector ($\boldsymbol{S}_a$, $\boldsymbol{S}_b$, $\boldsymbol{S}_c$) is generated using the commutation table (Table 2) [4, 15].

4 Simulation results

Various simulations were performed using MATLAB/Simulink [16] Figs. 10 to 25 evaluate the proposed approaches. The parameters used for these tests are presented in Table 3.

The results of Shunt Active Power Filter (SAPF) simulation controlled by the ZDPC, equipped with conventional PI and fuzzy MPPT, operating under balanced power supply, are shown in Figs. 10 to 26.

Fig. 10 shows all the simulated cases together during the time (0–1), in the first line we see the undistorted and distorted three-phase source voltages (V_{sabc}); the second line shows the change of irradiation with three levels (0, 600, 1000); the third line shows the load current in a single phase (I_{la}) without any change; the fourth line shows the different states of the filter currents before and after the activation of the active filter for the different cases of the source voltage (V_{sabc}) and the different states of the irradiation (I_{rad}); the last line shows the efficiency of the active filter which compensates for the harmonics generated by the polluting

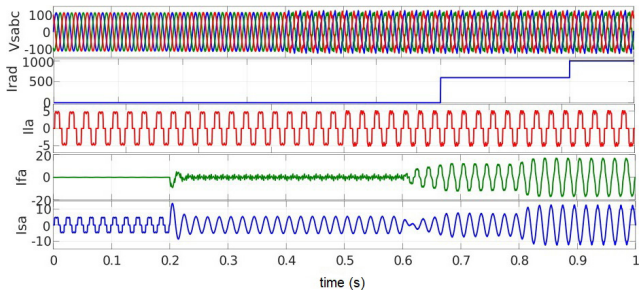

Fig. 10 simulation signals in the different cases

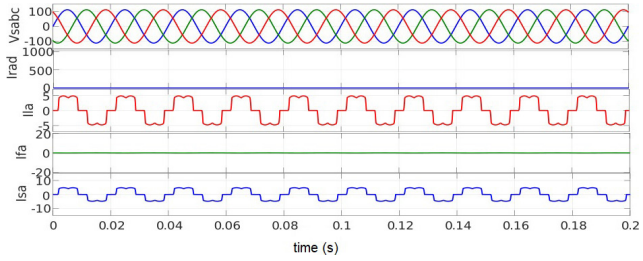

Fig. 11 Simulation signals in the absence of the filter and of irradiation

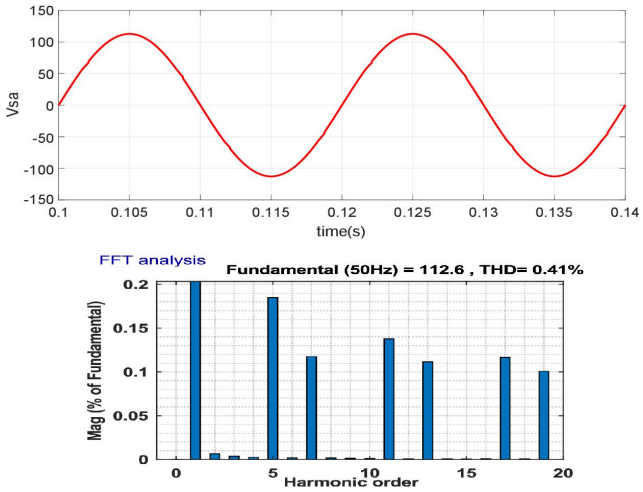

Fig. 12 Source voltage with his THD

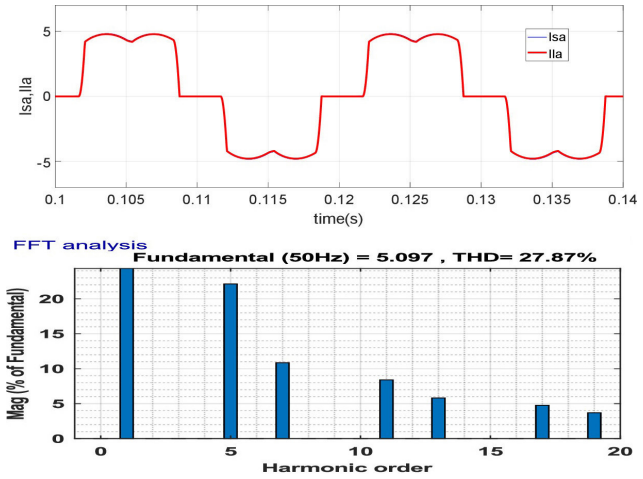

Fig. 13 Source current and load current with their THD

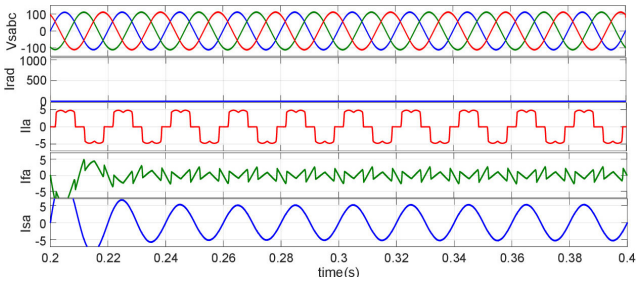

Fig. 14 Simulation signals with not distorded voltage source after the activation of the APF and in absence of irradiation

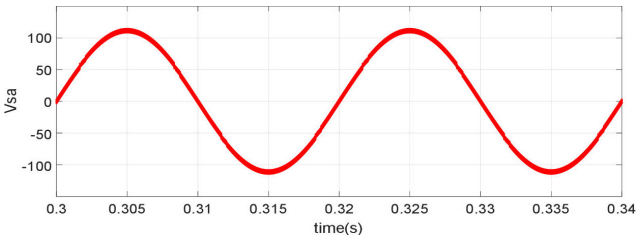

Fig. 15 Source voltage after activation of the APF

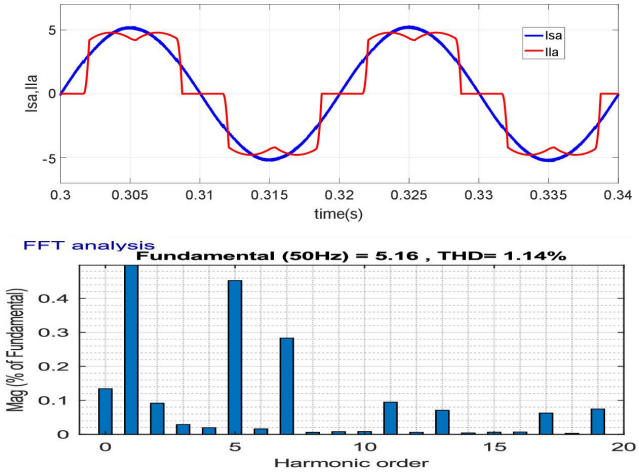

Fig. 16 Source current with his THD and the load current

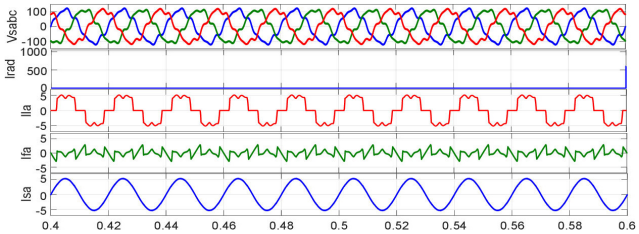

Fig. 17 Simulation signals with distorted voltage source after the activation of the APF and in absence of irradiation

load and makes the source current (I_{sa}) sinusoidal; and the increase in the value of the source current (I_{sa}) ensured by the PV system according to the value of the irradiation.

Fig. 11 zooms the signals in the time interval (0–0.2) where the filter is not activated and in the absence of irradiation (absence of energy injection towards the network),

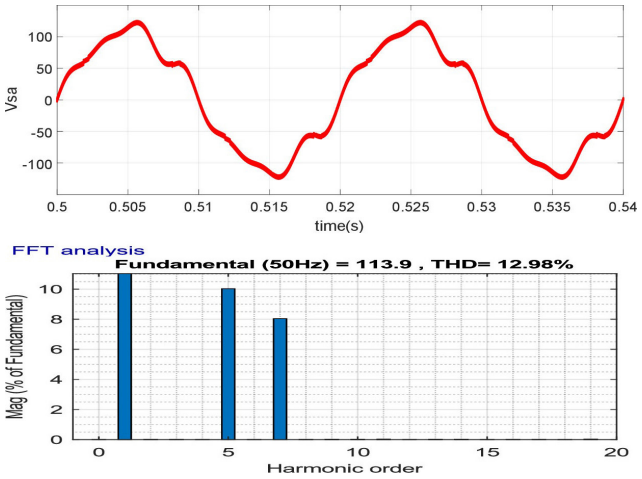

Fig. 18 Source voltage with his THD after activation of the APF

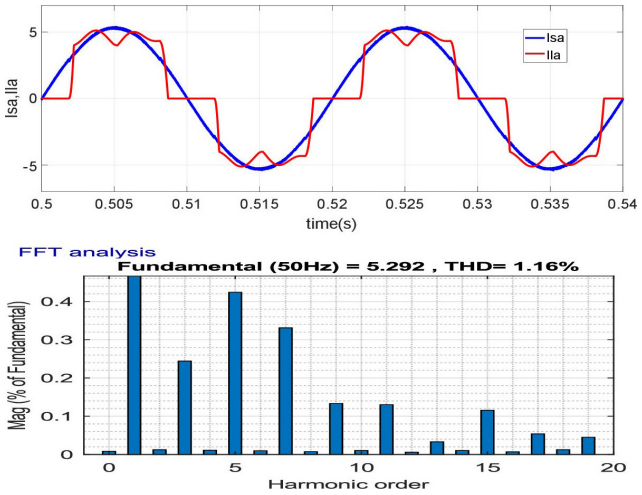

Fig. 19 Source current with his THD and the load current

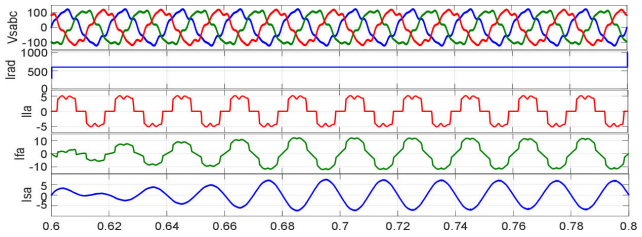

Fig. 20 Simulation signals after the activation of the APF and with the presence of irradiation and distorted source voltage

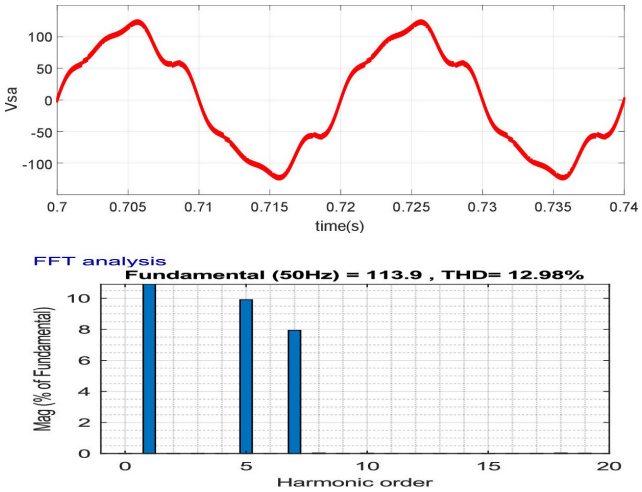

Fig. 21 Source voltage with his THD after activation of the APF

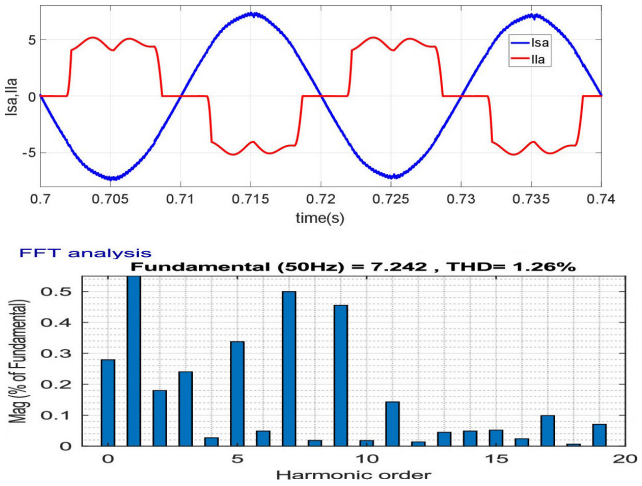

Fig. 22 Source current with his THD and the load current

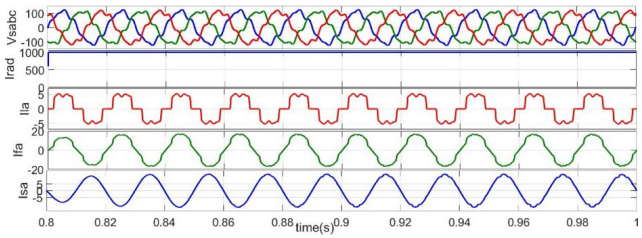

Fig. 23 Simulation signals after the activation of the APF and with the presence of max irradiation and distorded source voltage

in this case we note that the load current and the source current are the same as shown in Fig. 11.

Figs. 12 to 13 show the source voltage before distortion as well as the source current and their THDs.

Fig. 13 shows the source current and the load current of phase (*a*) (I_{sa}, I_{ca}) identical with a THD (27.87%) which means that the source current is highly distorted.

Fig. 14 shows the signals after the activation of the APF and still in the absence of irradiation during the time interval (0.2–0.4) with the undistorted source voltage, we notice the source current is corrected and becomes sinusoidal.

Fig. 15 shows the source voltage before distortion it is always sinusoidal.

We note that in Fig. 16 the source current resumes its sinusoidal form with a THD = 1.14% and in phase with the load current.

Fig. 17 shows the signals after APF activation and still in the absence of irradiation for the time interval (0.4–0.6);

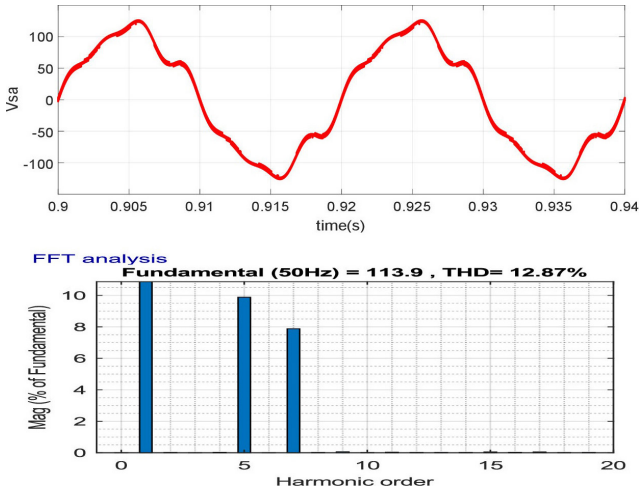

Fig. 24 Source voltage with his THD after activation of the APF

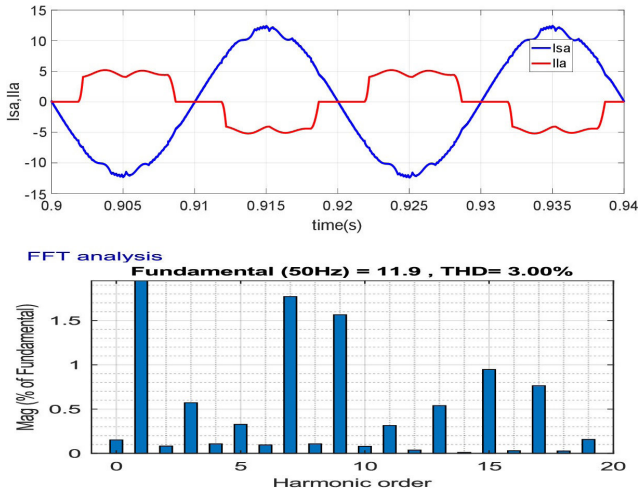

Fig. 25 Source current with his THD and the load current

Table 3 Simulation parameters

Parameters	Values with dimensions
V_s, F_s	80 V, 50 Hz
F switching (DC/AC Active Power Filter (APF) converter)	20 KHz
L_s, R_s	0.1 mH, 0.1 Ω
L_l, R_l	0.566 mH, 0.01 Ω
L_f, R_f, C_{DC}	2.5 mH, 0.01 Ω, 2200 µF
L, R	10 mH, 40 Ω
C_{pv}, L_{pv}	20 µF, 3 mH
DC bus voltage reference (V_{cref})	235 V
F switching (DC/DC boost converter)	5 kHz
N, ω_b, ω_h	2, 10^{-2} rad/s, 10^2 rad/s

we notice the source current is sinusoidal despite the source voltage is distorted.

Fig. 18 shows the source voltage after distortion and its frequency spectrum with 12.88% THD after APF activation.

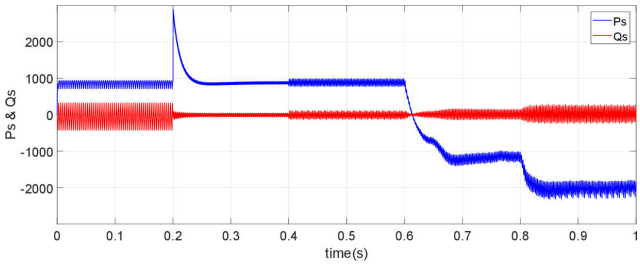

Fig. 26 Energy of the network in the different discussed cases

We see in Fig. 19 the source current is corrected and resumes its sinusoidal shape different from that of the load current, but they are in phase, the THD of the source current is 1.18%.

Fig. 20 presents the simulation signals during the activation of the APF and the injection of energy on the network, this in the time interval (0.6–0.8) where the source voltage is distorted.

In this case, the source current changes direction towards the network and becomes in phase opposition with the load current, which illustrates that the network becomes a receiver. The source current has a THD = 1.26% although the source voltage is distorted with a THD = 12.98%.

Fig. 21 shows the source voltage after distortion and its frequency spectrum with 12.88% THD after APF activation.

Fig. 22 clearly and simultaneously shows the role of the APF in compensating for the harmonics of the source current which becomes sinusoidal with a THD of 1.26% and the role of the PV panel which injects energy into the electrical network, this which explains the phase change of the source current by 180°.

Fig. 23 presents the simulation signals during the activation of the APF and the injection of energy to the network, this in the time interval (0.8–1) where the voltage source is distorted, in this case the irradiation is maximum (1000 w/m^2) and we notice the increase in the source current injected by the PV system.

Fig. 24 shows the distorted source voltage with a THD of 12.98%.

We note in Fig. 25 the increase in the source current which corresponds to a maximum value of the irradiation with a THD of 3.00%.

Fig. 26 shows the evolution of the energy of the network in the various cases discussed:

- Case 1: before activation of the APF and in the absence of irradiation withe the source voltage not distorted in interval [0, 0.2].
- Case 2: after activation of the APF and in the absence of irradiation with source voltage not distorted in interval [0.2, 0.4].

- Case 3: after activation of the APF and in the absence of irradiation withe source voltage distorted in interval [0.4, 0.6].
- Case 4: after the activation of the APF and in the presence of the irradiation withe source voltage distorted in interval [0.6, 0.8], we notice the active energy changes its direction towards the network electric which becomes receiver under the effect of the PV panel.
- Case 5: when switching from irradiation to the max (1000 w/m²), the increase in active energy corresponding to this irradiation is noted in interval [0.8, 1].

5 Conclusion

Conclusion. In this article, we studied a PV system controlled by a fuzzy command to inject energy into the network and improve the quality of the energy using an active power filter (SAPF). A new DPC technique named ZDPC, suitable for harmonic and reactive power compensation, has been proposed; HSF filters are used to separate harmonic currents and voltages causing power quality degradation on the network. Simulation results under various source voltage conditions confirm the good performance of the proposed approach.

References

[1] Benlahbib, B., Bouarroudj, N., Mekhilef, S., Abdelkrim, T., Lakhdari, A., Bouchafaa, F. "A Fuzzy Logic Controller Based on Maximum Power Point Tracking Algorithm for Partially Shaded PV Array-Experimental Validation", Electronika ir Electrotechnika, 24(4), pp. 38–44, 2018. https://doi.org/10.5755/j01.eie.24.4.21476

[2] Boudechiche, G., Sarra, M., Aissa, O., Gaubert, J.-P. "An investigation of solar active power filter based on direct power control for voltage quality and energy transfer in grid-tied photovoltaic system under unbalanced and distorted conditions", Journal of Engineering Research, 9(3B), pp. 168–188, 2021. https://doi.org/10.36909/jer.v9i3B.9061

[3] Boukezata, B., Chaoui, A., Gaubert, J.-P., Hachemi, M. "An improved fuzzy logic control MPPT based P&O method to solve fast irradiation change problem", Journal of Renewable and Sustainable Energy, 8(4), 043505, 2016. https://doi.org/10.1063/1.4960409

[4] Djazia, K., Krim, F., Chaoui, A., Sarra, M. "Active Power Filtering Using the ZDPC Method under Unbalanced and Distorted Grid Voltage Conditions", Energies, 8(3), pp. 1584–1605, 2015. https://doi.org/10.3390/en8031584

[5] Baazouzi, K., Bensalah, A. D., Drid, S., Chrifi-Alaoui, L. "Passivity voltage based control of the boost power converter used in photovoltaic system", Electrical Engineering & Electromechanics, 2, pp. 11–17, 2022. https://doi.org/10.20998/2074-272X.2022.2.02

[6] Sai Thrinath, B. V., Prabhu, S., Meghya Nayak, B. "Power quality improvement by using photovoltaic based shunt active harmonic filter with Z-source inverter converter", Electrical Engineering & Electromechanics, 6, pp. 35–41, 2022. https://doi.org/10.20998/2074-272X.2022.6.06

[7] Manoharan, P., Subramaniam, U., Babu, T. S., Padmanaban, S., Holm-Nielsen, J. B., Mitolo, M., Ravichandran, S. "Improved Perturb and Observation Maximum Power Point Tracking Technique for Solar Photovoltaic Power Generation Systems", IEEE Systems Journal, 15(2), pp. 3024–3035, 2021. https://doi.org/10.1109/JSYST.2020.3003255

[8] Kumar, A., Kumar, P. "Power Quality Improvement for Grid-connected PV System Based on Distribution Static Compensator with Fuzzy Logic Controller and UVT/ADALINE-based Least Mean Square Controller", Journal of Modern Power Systems and Clean Energy, 9(6), pp. 1289–1299, 2021. https://doi.org/10.35833/MPCE.2021.000285

[9] Altin, N., Ozdemir, S. "Three-phase three-level grid interactive inverter with fuzzy logic based maximum power point tracking controller", Energy Conversion and Management, 69, pp. 17–26, 2013. https://doi.org/10.1016/j.enconman.2013.01.012

[10] Verma, N., Jain, A., Nishi, Ahuja, H., Singh, G. "Maximum Power Point Tracking MPPT Methods for Photovoltaic Modules", In: 2021 International Conference on Advance Computing and Innovative Technologies in Engineering (ICACITE), Greater Noida, India, 2021, pp. 223–227. ISBN 978-1-7281-7742-7 https://doi.org/10.1109/ICACITE51222.2021.9404571

[11] Chavan, U. M., Thorat, A. R., Bhosale, S. S. "Shunt Active Filter for Harmonic Compensation Using Fuzzy Logic Technique", In: 2018 International Conference on Current Trends towards Converging Technologies (ICCTCT), Coimbatore, India, 2018, pp. 1–6. ISBN 978-1-5386-3703-6 https://doi.org/10.1109/ICCTCT.2018.8550962

[12] Tareen, W. U., Mekhilef, S., Seyedmahmoudian, M., Horan, B. "Active power filter (APF) for mitigation of power quality issues in grid integration of wind and photovoltaic energy conversion system", Renewable and Sustainable Energy Reviews, 70, pp. 635–655, 2017. https://doi.org/10.1016/j.rser.2016.11.091

[13] Bengourina, M. R., Rahli, M., Slami, S., Hassaine, L. "PSO based direct power control for a multifunctional grid connected photovoltaic system", International Journal of Power Electronics and Drive System (IJPEDS), 9(2), pp. 610–621, 2018. https://doi.org/10.11591/ijpeds.v9.i2.pp610-621

[14] Aissa, O., Moulahoum, S., Colak, I., Kabache, N., Babes, B. "Improved performance and power quality of direct torque control of asynchronous motor by using intelligent controllers", Electric Power Components and Systems, 44(4), pp. 343–358, 2016. https://doi.org/10.1080/15325008.2015.1117541

[15] Mesbahi, N., Ouari, A., Ould Abdeslam, D., Djamah, T., Omeiri, A. "Direct power control of shunt active filter using high selectivity filter (HSF) under distorted or unbalanced conditions", Electric Power Systems Research, 108, pp. 113–123, 2014. https://doi.org/10.1016/j.epsr.2013.11.006

[16] MathWorks "MATLAB/Simulink, R2017b", Available at: https://matlab.mathworks.com [Accessed: 21 October 2022]